Aalborg Universitet

A Control Method for Converter-interfaced Sources to Improve Operation of Directional Protection Elements

Yang, Zhe; Liu, Zhou; Zhang, Qi; Chen, Zhe; Jesus Chavez, Jose de ; Popov, Marjan

A Control Method for Converter-interfaced Sources to Improve Operation of Directional Protection Elements

Zhe Yang, *Student Member, IEEE*, Zhou Liu, *Senior Member, IEEE*, Qi Zhang, *Student Member, IEEE*, Zhe Chen, *Fellow, IEEE*, Jose de Jesus Chavez*, Member, IEEE* and Marjan Popov, *Fellow, IEEE*

Abstract—The traditional fault control strategy of converter-interfaced renewable energy sources (CIRESs) may bring about a lower sensitivity level or misoperation of fault component-based directional elements. To overcome this problem, a new control scheme is proposed to adjust sequence impedance angles of CIRESs by computing suitable current references of the CIRES controller. Meanwhile, these current references are maximized by an iterative algorithm to make full use of the short-circuit capacity of CIRESs. The proposed control scheme is applicable to various faulty conditions such as different fault types, power factors, weak grids, and larger fault resistances. Compared with the new directional elements that need to update protection algorithms, the proposed control strategies can make CIRESs compatible with the existing directional elements whilst the necessary fault ride-through (FRT) requirements can still be satisfied. Furthermore, all the controller parameters are not required to be revised based on the detected fault type, even with only local measured data collected. The associated PSCAD simulations, real-time digital simulator (RTDS) testing and the downscale hardware experiment verify the proposed method.

*Index Term*s—converter-interfaced renewable energy sources, directional elements, fault ride through, impedance angle.

I. INTRODUCTION

Renewable energy sources (RESs) are integrated into the power system with a high permeability to mitigate energy crisis and climate change [1-2]. Unlike synchronous generators (SGs), converter-interfaced RESs (CIRESs), such as photovoltaic (PV) and permanent magnet synchronous generators (PMSGs), are connected to the grid through full-power inverters [3]. Their impedance characteristics are different from those of SGs, which may affect the correct operation of the traditional fault component-based directional elements [4]. Fault component-based directional elements are the key element of directional pilot protection, so their misoperation/failure will seriously jeopardize the security and stability of the grid

[5-6].

In traditional transmission networks, fault component-based directional elements have an excellent performance owing to the stable sequence impedance angles of SGs. However, sequence impedance angles of CIRESs will change within a large scope in different fault scenarios [6-7]. It has been pointed out in [8] that unstable sequence impedances would seriously affect the performance of fault component-based directional elements, but the analytical expression of the CIRES sequence impedances and the related theoretical analysis are not provided. The mathematical expressions were derived in [9] combined with the fault currents of CIRESs in the ABC frame, and extensive simulation verifications were conducted under different fault conditions. In [10], CIRESs are represented by a controllable current source instead of a voltage source with a constant impedance like SGs. Therefore, the directional elements based on the impedance feature of SGs will be affected when CIRESs are connected. In [11], a hardware-in-the-loop (HIL) experiment for negative-sequence directional elements was performed, and a similar conclusion was obtained. In addition, for negative-sequence directional elements on the grid side, it could report a forward direction for reverse faults, which would affect the grid security [12].

In order to improve the protection performance, some new solutions have been proposed, and they can be divided into three groups, i.e. time domain-based methods, frequency domain-based methods, and active control-based methods. For time-domain methods, the least square method was used in [13-14] to fit the equivalent resistance in the time-domain differential equation, and the resistance sign was utilized to determine the fault direction. To deal with the voltage dead zone for the fault at the relay output, an auxiliary criterion using the correlation between the computed voltage drop and the measured voltage drop was added in [15]. However, the current waveform was seriously distorted by the current limiter in the first quarter cycle during the fault inception, so the performance of these time-domain directional elements was slightly poor [16]. Another time-domain method was proposed in [17] using the transient energy difference between forward and reverse faults, but this method based on traveling waves required a high sampling frequency. For frequency-domain methods, the fault direction was distinguished using the current magnitude difference because the short-circuit current of SGs would be much larger than that of CIRESs [18]. In [10], it was reported that sequence impedance magnitudes of CIRESs were much higher than those of SGs, hence a new directional element using this feature was put forward. The researchers in [9] came up with a directional element in reliance on the high-frequency impedance model of CIRESs, but the available frequency range should be further

studied. In addition, the negative-sequence current threshold was increased to enhance the security of negative-sequence directional elements [19]. However, all the protection devices in the vicinity of CIRESs need to be updated to implement the previous methods, which would result in a significant cost increase. Therefore, some researchers try making fault characteristics of CIRESs behave like those of SGs to ensure the correct operation of original directional elements by adjusting the control system of CIRESs, which can be also called active control-based methods. The negative-sequence voltage was controlled to zero in a new dual current controller in [20]. Here, reasonable negative-sequence impedance parameters were designed considering protection requirements. Similarly, in [21], it was pointed out that negative-sequence directional elements could operate correctly near sources that comply with the latest version of the standard VDE-AR-N 4120. However, neither of the two methods controls the angle of the apparent positive-sequence impedance derived from the incremental voltage and current. A control method was used in [22] to make CIRESs equivalent to a virtual voltage source with a virtual impedance in the positive-sequence fault circuit. However, the apparent impedance angle seen by the positive-sequence fault component-based directional elements (denoted by positive-sequence directional elements in the following content) could not be adjusted since it is related to the electric quantities before the fault. Meanwhile, some controller parameters need to be tuned according to different fault types, so a new phase selector reported in [23] is also required. Therefore, more work about active control is needed.

In this paper, a new control-based method is proposed for the direction detection with the following contributions: 1) the impedance angle detected by positive-sequence directional elements is adjusted to be -90° for forward faults such that positive-sequence directional elements can operate correctly. 2) All the controller parameters are not necessary to be changed according to different fault types whilst important fault ride through (FRT) requirements can be achieved. 3) It can show good performances for high resistance faults and operate in weak grids accordingly, and is applicable under different fault types, power ratings and power factors before the fault.

The remainder of this paper is organized as follows. Section II presents the examined topology and analyzes the present challenges of the directional elements when CIRESs are connected. Thereafter, a new control strategy is proposed in Section III to adjust sequence impedance angles of CIRESs to make directional elements work properly. A PSCAD simulation analysis is done in Section IV, and real-time digital simulator (RTDS) experiment and downscale hardware experiment are also performed to verify the proposed method in Section V and Section VI respectively. In addition, the shortcomings of the proposed method are discussed in Section VII. Finally, the conclusions are summarized in Section VIII.

II. PROBLEM STATEMENT

This section will analyze the fault current behavior of CIRESs and clarify why directional elements nearby experience low sensitivity and may fail to operate.

A. The fault current of CIRESs

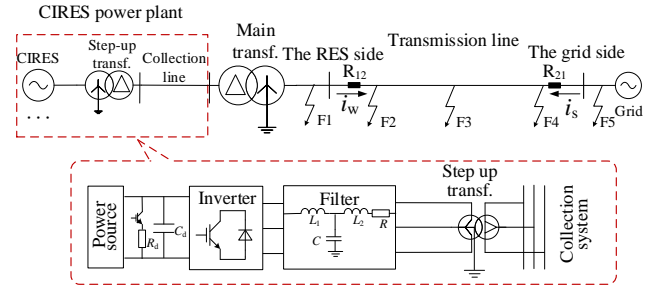A typical structure for the transmission line with CIRESs

Fig. 1.   The transmission line with CIRESs.

is illustrated in Fig. 1. CIRESs are integrated into the collection system by three-phase two-level power inverters, and the produced electricity will be sent to the remote grid through an overhead line after the main transformer raises the voltage. Fault point F1 is located at the left side of the RES-side bus. The other four fault points F2, F3, F4, and F5 are respectively set at 0%, 50%, 100% of the transmission line and the exit of the downstream line. Directional elements are deployed at R_{12} and R_{21}.

For CIRESs, a double current loop controller based on sequence decoupling is adopted with a voltage vector oriented to the positive-sequence D axis (Q axis leads D axis), and the point of common coupling (PCC) is placed at the RES-side bus [24]. The positive- and negative-sequence separation is achieved by delaying one-quarter of a cycle method (5 ms for the power frequency of 50 Hz) in the $\alpha\beta$ frame [25]. Since the fault features of CIRESs are mainly determined by the grid-side inverter, RESs with their source-side converter can be substituted by a controllable current source [26]. To avoid overvoltage on the DC side, a chopper circuit is installed between the two terminals of the DC capacitor. During normal operation, a constant DC voltage control is used to produce the positive-sequence D-axis current reference, and other current references are set to 0, so CIRESs operate at the unity power factor. Once a fault occurs, these current references will be set directly according to specific fault ride-through (FRT) requirements.

In this case, the phase-A positive-sequence fault current during the fault steady state can be written as [27]:

$$i_{a1} = \sqrt{i_{1dref}^2 + i_{1qref}^2}\, \sin\left(\omega t + \theta_{1p} + \arctan\left(\frac{i_{1qref}}{i_{1dref}} \right) + 90^\circ \right) \quad (1)$$

where i_{1dref} and i_{1qref} are positive-sequence DQ-axis current references, θ_{1p} is the phase-locked angle, ω is the synchronous angular velocity, and t is the time variable.

It can be found from (1) that the magnitude and the phase angle of the positive-sequence current can be controlled by i_{1dref} and i_{1qref}. Similarly, the negative-sequence current is controlled by negative-sequence current references during the fault steady state, so the phase-A negative-sequence current is expressed as:

$$i_{a2} = \sqrt{i_{2dref}^2 + i_{2qref}^2}\, \sin\left(\omega t - \theta_{2p} - \arctan\left(\frac{i_{2qref}}{i_{2dref}} \right) + 90^\circ \right) \quad (2)$$

where i_{2dref} and i_{2qref} are negative-sequence DQ-axis current references, and θ_{2p} is equal to minus θ_{1p}.

B. Positive- and negative-sequence directional elements

After the controlled feature of the CIRES fault current is revealed, the performance of positive- and negative-sequence directional elements can be analyzed. Both can identify the fault direction by computing the apparent impedances, Z_1 and Z_2 [8, 10]:
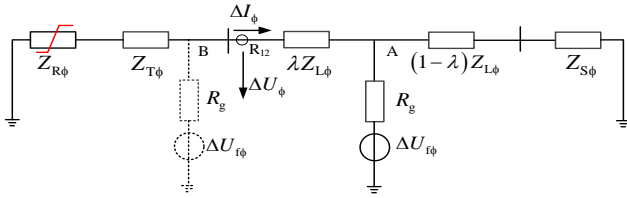
Fig. 2. Sequence fault component networks.

$$Z_1 = \frac{\Delta U_1}{\Delta I_1} = \frac{U_1 - U_b}{I_1 - I_b} \qquad (3)$$

$$Z_2 = \frac{\Delta U_2}{\Delta I_2} = \frac{U_2}{I_2} \qquad (4)$$

where Δ denotes the superimposed components that are equal to the post-fault components minus the pre-fault components, U and I are the voltage and current phasors measured at the relay point. Subscripts 1 and 2 denote positive- and negative-sequence components during the fault, and b denotes the electric quantities before the fault.

In general, the electric quantities before the fault only include positive-sequence components [18], so ΔU_2 in (4) is equal to U_2. According to the reference positive direction from the busbar to the line, the impedance angle detected by directional elements should approach -90° for forward faults in the traditional grid [9]. Therefore, the criterion of fault component-based directional elements for forward faults is usually expressed as (5) [8], and the closer the apparent impedance angle is to -90°, the higher the sensitivity of the directional element will be.

$$-180° < \angle Z_\phi < 0° \qquad (5)$$

where $\angle$ denotes the phase angle of a phasor, and ϕ denotes the sequence number, 1, 2 or 0.

For the positive- and negative-sequence fault component network in Fig. 2, Z_R is the equivalent impedance of the CIRES power plant, Z_T, Z_L and Z_S are the sequence impedances of the main transformer, the transmission line and the grid, λ denotes the ratio of the line impedance between the fault point and the relay point to the total line impedance. R_g is the fault resistance, and ΔU_f is the voltage superimposed component at the fault point. In addition, the 220 kV transmission line connected to CIRESs is usually less than 100 km, so the line capacitive current is usually so small that it is neglected [28].

When the fault is located at A, the apparent impedance Z_ϕ measured at R_{12} is computed as (6):

$$Z_\phi = -\left(Z_{R\phi} + Z_{T\phi}\right) \qquad (6)$$

Since $Z_{R\phi}$ is much larger than $Z_{T\phi}$, the phase angle of Z_ϕ depends on the phase angle of $Z_{R\phi}$. Unlike sequence impedance angles of SGs, which are always close to 90° due to the fixed magnetic loop, the impedance angle of CIRESs is variable with the current control references since they determine the magnitude and the angle of I_1 and I_2 in (3) and (4). During a fault, in order to improve the grid voltage, the positive-sequence Q-axis current reference (reactive current) is usually provided according to voltage sags, and the left room is utilized to generate the positive-sequence D-axis current reference. In addition, negative-sequence current references are usually set to 0 [23]. However, the impedance angle adjustment of CIRESs is not considered in these

traditional FRT strategies, so positive-sequence directional elements may misjudge the fault direction.

When the fault point is at B in Fig. 2, the apparent impedance Z_ϕ detected at R_{12} will be:

$$Z_\phi = Z_{L\phi} + Z_{S\phi} \qquad (7)$$

At this time, the phase angle of Z_ϕ is determined by the impedance angle of the transmission line and the equivalent grid, which is a constant about 90°, so positive- and negative-sequence directional elements can correctly determine the reverse faults.

Conversely, positive- and negative-sequence directional elements at R_{21} can declare a forward fault for a reverse fault at F5 since the apparent impedance is equal to $Z_{R\phi}+Z_{T\phi}+Z_{L\phi}$, so the security of the grid could be seriously undermined.

C. Zero-sequence directional elements

Similarly, the apparent impedance Z_0 is defined as [9]:

$$Z_0 = \frac{U_0}{I_0} \qquad (8)$$

where subscript 0 represents the zero-sequence component.

For an asymmetrical ground fault on the line, Z_0 is always equal to $-Z_{T0}$ due to the Y_nD neutral point of the main transformer, which has nothing to do with the equivalent impedance of CIRESs, so the performance of ZSDEs is not adversely affected by CIRESs. However, it should be noted that ZSDEs are only applicable for asymmetrical ground faults, so it is necessary to improve the performance of positive- and negative-sequence directional elements to detect the fault direction for phase-to-phase faults and three-phase faults.

In conclusion, the traditional FRT strategies of CIRESs will adversely affect the performance of positive- and negative-sequence directional elements, but zero-sequence directional elements are still effective for asymmetrical ground faults.

D. Case studies

The Danish FRT strategy in Fig. 3 (a) is used to evaluate the performance of directional elements. i_{1qref} is determined according to voltage sags [29], and i_{1dref} is computed using $\sqrt{\gamma^2 - i_{1qref}^2}$. For negative-sequence current references, they are usually set to 0. In area A, CIRESs work in normal conditions; in area B, they should be connected to the grid for the defined time, as displayed in Fig. 3 (b); and in area C, they are allowed to disconnect from the grid.

When γ is set to 1.5, and a metallic phase-A ground fault appears at F2 in Fig. 1, the related measurements of positive- and negative-sequence directional elements can be observed in Fig. 4.

The computed current angle in Fig. 4 (a) essentially coincides with the actual value during the steady state fault,
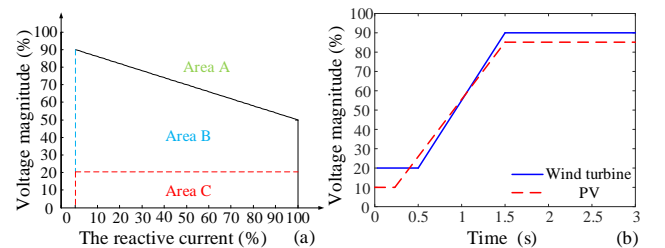

Fig. 3. FRT requirement in Denmark. (a) Reactive current, (b) the time-voltage profile.
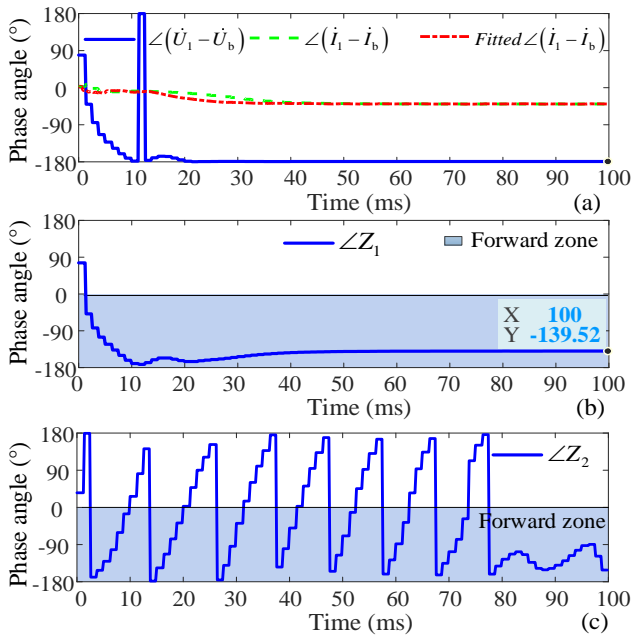
Fig. 4. The related measurements of directional elements under Danish FRT strategies. (a) Voltage and current, (b) $\angle Z_1$, (c) $\angle Z_2$.

which proves that the positive-sequence fault current is well controlled by positive-sequence current references, and the error during the transient process derives from the phase-locked loop error. At this time, the impedance angle measured by positive-sequence directional elements in Fig. 4 (b) is stable at -139.52° with a large deviation from -90° at 0.5 s, so the elements are with low sensitivity. Meanwhile, the phase angle of Z_2 in Fig. 4 (c) will vary within a large scope since the negative-sequence current angle is unpredictable according to (2) when i_{2dref} and i_{2qref} are set to 0, which will lead to the wrong direction identification. In some commercial directional elements, the overcurrent supervision function is added. In this regard, negative-sequence directional elements cannot be activated to determine the fault direction if no negative-sequence current is injected [12].

III. CONTROL-BASED SOLUTION

In order to adjust sequence impedance angles of CIRESs to make directional elements operate correctly, suitable current references are calculated considering the requirements of line protection and FRT.

A. Positive-sequence current references

To compute suitable current references to ensure the correct operation of positive-sequence directional elements for forward faults, the corresponding CIRES fault current angle should be derived from related protection principles. Therefore, positive-sequence voltage and current phasors at the relay point during and before the fault are firstly expressed as:

$$\begin{cases} U_1 = |U_1| \angle \varphi_1 \\ U_b = |U_b| \angle \varphi_b \end{cases}, \begin{cases} I_1 = |I_1| \angle \alpha_1 \\ I_b = |I_b| \angle \alpha_b \end{cases} \qquad (9)$$

where φ and α are the voltage angle and the current angle.

Substituting (9) into (3), the expression of Z_1 can yield:

$$Z_1 = \frac{|U_1|\cos\varphi_1 - |U_b|\cos\varphi_b + j(|U_1|\sin\varphi_1 - |U_b|\sin\varphi_b)}{|I_1|\cos\alpha_1 - |I_b|\cos\alpha_b + j(|I_1|\sin\alpha_1 - |I_b|\sin\alpha_b)} \qquad (10)$$

Based on this, the magnitude and the phase angle of Z_1 can be obtained by (11) and (12):

$$|Z_1| = \frac{\sqrt{(|U_1|\cos\varphi_1 - |U_b|\cos\varphi_b)^2 + (|U_1|\sin\varphi_1 - |U_b|\sin\varphi_b)^2}}{\sqrt{(|I_1|\cos\alpha_1 - |I_b|\cos\alpha_b)^2 + (|I_1|\sin\alpha_1 - |I_b|\sin\alpha_b)^2}} \qquad (11)$$

$$= \sqrt{\frac{A_1^2 + B_1^2}{A_2^2 + B_2^2}}$$

$$\angle Z_1 = \arctan\frac{B_1}{A_1} - \arctan\frac{B_2}{A_2} \qquad (12)$$

where $\arctan(\cdot)$ is defined to be between -180° and 180°, and $|\cdot|$ denotes the magnitude of a phasor. Additionally, $A_1 = |U_1|\cos\varphi_1 - |U_b|\cos\varphi_b$, $A_2 = |I_1|\cos\alpha_1 - |I_b|\cos\alpha_b$, $B_1 = |U_1|\sin\varphi_1 - |U_b|\sin\varphi_b$, and $B_2 = |I_1|\sin\alpha_1 - |I_b|\sin\alpha_b$.

Let (12) equal to -90° to ensure the correct operation of the directional element, so the required phase angle of I_1 can be calculated:

$$\alpha_1 = \arcsin\frac{F}{\sqrt{1 + (\tan E)^2}} + E \qquad (13)$$

where E and F are:

$$E = \arctan\frac{B_1}{A_1} + 90° \qquad (14)$$

$$F = \frac{|I_b|}{|I_1|}\sin\alpha_b - \frac{|I_b|}{|I_1|}\tan E \cdot \cos\alpha_b \qquad (15)$$

The magnitude of I_1 in (15) can be obtained by considering the current limiting of the inverters, which will be discussed in Section III. C. After obtaining this required phase angle, the first constraint for the positive-sequence current references can be obtained by combining (1) with (13):

$$k_1 = \frac{i_{1qref}}{i_{1dref}} = \tan\left(\alpha_1 - 90° - \theta_{1p}\right) \qquad (16)$$

In addition, the positive-sequence current peak value I_{1m} is equal to $\sqrt{i_{1dref}^2 + i_{1qref}^2}$ according to (1). Therefore, two current references can be calculated, as shown in (17):

$$\begin{cases} i_{1dref} = \sqrt{\frac{1}{1 + k_1^2}} I_{1m} \\ i_{1qref} = k_1 i_{1dref} \end{cases} \qquad (17)$$

When current references are set according to (17), the directional element can operate correctly for forward faults since the impedance angle seen by them will be close to -90°. In addition, some commercial directional elements also check the apparent impedance magnitude, but this is usually satisfied since CIRESs are weak sources [12].

B. Negative-sequence current reference values

The apparent impedance angle of negative-sequence directional elements can also be adjusted by designing suitable negative-sequence current reference values. In order to determine the corresponding negative-sequence current angle, the negative-sequence components at the relay point are firstly expressed in the form of phasors:

$$\begin{cases} U_2 = |U_2| \angle \varphi_2 \\ I_2 = |I_2| \angle \alpha_2 \end{cases} \qquad (18)$$

Substituting (18) into (4), the apparent impedance Z_2 can be computed as follows:

$$Z_2 = \frac{|U_2|}{|I_2|} \angle (\varphi_2 - \alpha_2) \qquad (19)$$

The impedance angle in (19) is only related to the phase angles of the negative-sequence voltage and the negative-sequence current during the fault. To ensure negative-sequence directional elements to operate correctly, let (19) equal -90°, so the required negative-sequence current angle can be obtained:

$$\alpha_2 = \varphi_2 + 90° \qquad (20)$$

By combining (2) and (20), the first constraint for negative-sequence current references yields:

$$k_2 = \frac{i_{2\text{qref}}}{i_{2\text{dref}}} = -\tan\left(\varphi_2 + \theta_{2\text{p}}\right) \qquad (21)$$

In addition, the negative-sequence current peak value $I_{2\text{m}}$ is equal to $\sqrt{i_{2\text{dref}}^2 + i_{2\text{qref}}^2}$ according to (2), so two negative-sequence current references can be obtained as follows:

$$\begin{cases} i_{2\text{dref}} = \sqrt{\dfrac{1}{1+k_2^2}} I_{2\text{m}} \\ i_{2\text{qref}} = k_2 i_{2\text{dref}} \end{cases} \qquad (22)$$

For the proposed method, all the parameters are unnecessary to be tuned according to different fault types, so the phase selector in [23] is not required, which is a big advantage compared with the method in [22].

C. Initial setting of sequence currents

To compute the current references in (17) and (22), suitable initial values of $I_{1\text{m}}$ and $I_{2\text{m}}$ must be given considering the current limiting of the inverter. In general, the maximum fault current is limited to 1.2 to 1.5 times the rated current [27,30], which is denoted as γI_N. Among them, γ is the current limiting multiple, and I_N is the rated current. Define a current variable I_{peak} that is equal to $|I_1|$ plus $|I_2|$, and assumed that $|I_2|$ is β times $|I_1|$, there is:

$$I_{\text{peak}} = |I_1| + |I_2| = (1+\beta)|I_1| \qquad (23)$$

By having (23) equal to γI_N, the initial values of $I_{1\text{m}}$ and $I_{2\text{m}}$ can be computed. After that, the corresponding current references can be computed. At this time, it can be expected that the actual fault current must be less than γI_N since the phase angle difference between positive- and negative-sequence currents is not considered in (23). To make full use of short-circuit capacities, the method to maximize fault currents will be discussed in Section III. D.

In addition, the range of β will be discussed as follows. If β is larger than 1, i.e., $|I_2|>|I_1|$, the phase rotation of the fault current from CIRESs will be changed from ABC to ACB, which will lead to various protection problems, so β must be smaller than 1. In addition, a certain amount of $|I_2|$ is also necessary to activate negative-sequence directional elements, so β can be chosen from 0.2 to 1 [22].
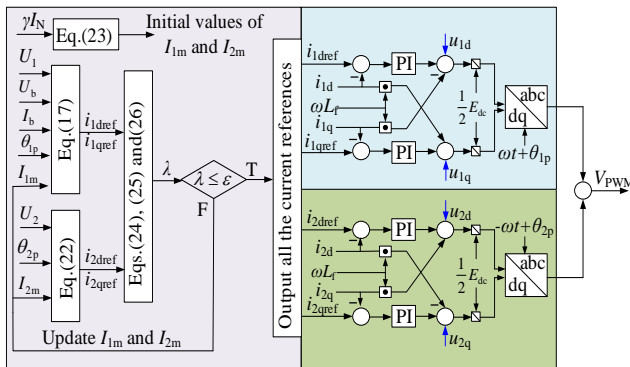
Fig. 5. The proposed control scheme.

D. Maximize current references

This part will discuss how to obtain the maximum allowable fault currents. Firstly, the Cosine theorem is used to calculate three-phase fault currents:

$$\begin{cases} |I_\text{a}| = \sqrt{|I_1|^2 + |I_2|^2 + 2|I_1||I_2|\cos\Delta\alpha} \\ |I_\text{b}| = \sqrt{|I_1|^2 + |I_2|^2 - 2|I_1||I_2|\cos(\Delta\alpha - 60°)} \\ |I_\text{c}| = \sqrt{|I_1|^2 + |I_2|^2 - 2|I_1||I_2|\cos(\Delta\alpha + 60°)} \end{cases} \qquad (24)$$

where $\Delta\alpha$ is the phase angle difference between positive- and negative-sequence currents for phase-A, which satisfies the following formula:

$$\Delta\alpha = \arctan\frac{i_{1\text{qref}}}{i_{1\text{dref}}} - \arctan\frac{i_{2\text{qref}}}{i_{2\text{dref}}} \qquad (25)$$

To obtain maximum current references, the following iterative computation method is adopted:

1) When the initial values of $|I_1|$ and $|I_2|$ are determined by (23), the related peak values $I_{1\text{m}}$ and $I_{2\text{m}}$ can be obtained.

2) The positive- and negative-sequence current references are obtained by (17) and (22), and then the three-phase currents can be calculated by (24) and (25).

3) When the maximum value of three-phase currents is still less than the current limiting value γI_N, $|I_1|$ will be increased by λ in (26) as the new initial value. If not, $|I_1|$ will be reduced by λ as the new initial value. After that, steps 2) and 3) will be repeated until λ converges to the given range, ε.

$$\lambda = \left| \max\left\{ |I_\text{a}|, |I_\text{b}|, |I_\text{c}| \right\} - \gamma I_\text{N} \right| \qquad (26)$$

By applying this method, the final current references can be obtained and provided to the current controller to make the output fault current reach the maximum value. It should be noted that the current references produced during the iteration process are not transmitted to the current controller, so the iteration algorithm and process do not impact the dynamic response of the control system.

In summary, the control diagram of this new strategy can be observed in Fig. 5. The D- and Q-axis current reference values already include a current limiting action in (23) and an explicit current limiting block is not needed in the diagram in Fig. 5. In addition, the $i_{1\text{qref}}$ is not determined based on the voltage sag, and therefore the $i_{1\text{qref}}$ value will not violate the current limits of the source. For the used controller in the right side, the DC voltage E_{dc} participates in the generation of the modulation wave V_{PWM}, so the fault signatures on the AC side is not affected by the transient process of the DC voltage [18]. The grid voltage (marked in blue) is feedforward compensated to avoid the impact of grid disturbances [20], and the coupling term is also added in the current control loop to realize DQ-axis decoupling [22]. In addition, positive- and negative-sequence current references are given by the above-mentioned iterative method, and PI parameters are tuned according to the suggested method in [31]:

$$\begin{cases} k_{\text{ip}} = \omega_\text{c} L_\text{f} \\ k_{\text{ii}} = \omega_\text{c} R_\text{f} \end{cases} \qquad (27)$$

where k_{ip} and k_{ii} are respectively the proportional coefficient and the integral coefficient, and ω_c denotes the cutoff frequency. L_f and R_f are the total inductance and the total resistance between the PCC and the inverter output.

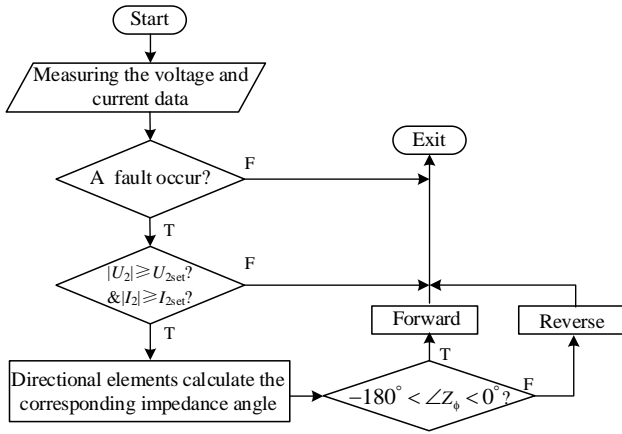The protection flow chart is shown in Fig. 6. Firstly, the

Fig. 6. The protection flow chart.

fault needs to be detected within several milliseconds, and the method in [32] can be used. After that, the negative-sequence voltage and current will be checked if both exceed their corresponding threshold values, U_{2set} and I_{2set}. U_{2set} can be set to 2% of the nominal voltage [23], and I_{2set} is set to 10% of the nominal current [12]. Finally, the impedance angle seen by directional elements is calculated using the data collected at the relay point. If the apparent impedance angle is located between -180° to 0°, a forward fault is determined; if not, a reverse fault is identified.

IV. SIMULATION ANALYSIS

The analysis is performed for a 100 MW CIRES power plant which is modeled in PSCAD. The transmission line is 40 km with a voltage level of 220 kV, the grid impedance is $0.1+j3.14 \, \Omega$, and the rest of the parameters are listed in Table A.I. At this time, the rated capacity of CIRESs is one-thirtieth of the short-circuit capacity of the grid detected at R_{12}. All the faults occur at 0 s, and CIRESs operate at the unity power factor during normal operation without a special illustration.

A. Simple case with the proposed control strategy

When the proposed method is performed in the same fault scenario as Fig. 4, the related measurements of positive- and
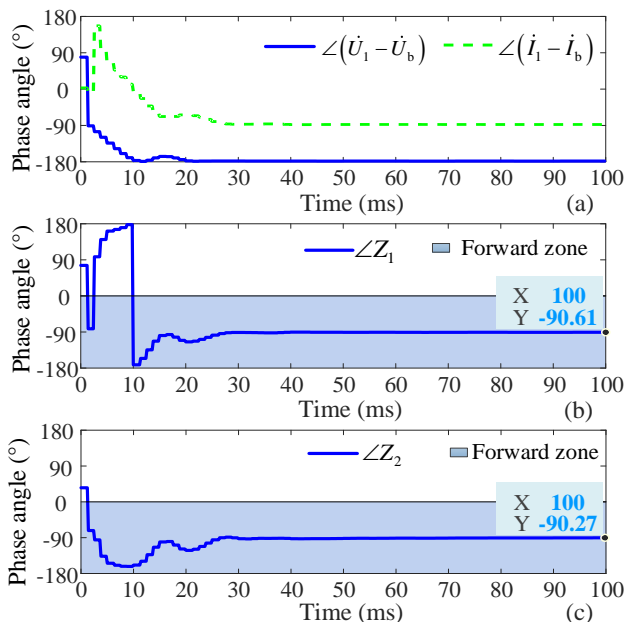
negative-sequence directional elements at R_{12} are depicted in Fig. 7. At this time, γ and β are taken as 1.5 and 0.3.

The measured current in Fig. 7 (a) is adjusted according to the measured voltage. At this time, the impedance angle computed by the positive-sequence directional elements in Fig. 7 (b) is stable at -90.61° at 500 ms, so its sensitivity has been greatly improved. However, since the control system needs some time to reach the steady state, the apparent impedance angle has a large fluctuation during the first 20 ms after the fault. Once the controller reaches the steady state, the phasor data window is filled with the stabilized samples, so the controller and phasor settling times appear in series. Therefore, a small time delay of 40 ms can be added in the protective algorithm to make sure that the transient impact can be avoided although this will reduce the speed of directional elements. Similarly, negative-sequence directional elements also perform well in Fig. 7 (c). Under this circumstance, i_{1dref} and i_{1qref} are equal to 1.0024 and -0.6800, which shows that CIRESs can inject reactive power into the grid to support the grid voltage. The positive-sequence voltage at PCC, active and reactive power values and three-phase currents at the inverter terminal are shown in Fig. 8.

The positive-sequence voltage at PCC in Fig. 8 (a) drops to 70.5% of the rated voltage. Regarding the FRT requirement in Fig. 5 (a), the operation state of CIRESs will be located at area A, so they can ride through the fault. In addition, the active power is reduced to 0.70 p.u., and the reactive power is increased to 0.62 p.u. in Fig. 8 (b), so CIRESs can provide support for the grid voltage. The proposed iterative algorithm converges after two or three iterations, and at this time, the phase-A current reaches the maximum allowable value (1.5 p.u.), as shown in Fig. 8 (c). Unlike SGs, the fault current for phase C is close to the maximum value, but the phase-B fault current is relatively small because the fault current from CIRESs depends on the specific control strategy instead of fault types.

B. Case study with different fault points and types

The proposed method is evaluated under different fault points and different fault types. The fault resistance is set to

Fig. 7. The related measurements of directional elements under the proposed control strategy. (a) Voltage and current, (b) $\angle Z_1$, (c) $\angle Z_2$.
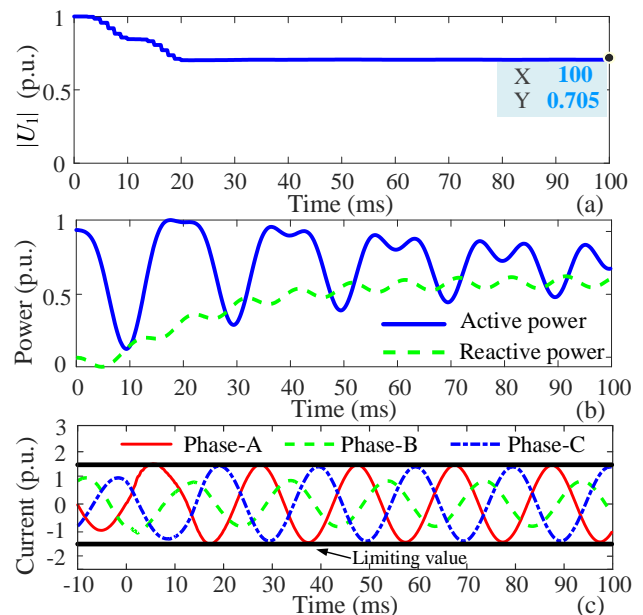

Fig. 8. The related measurement at PCC and the inverter terminal. (a) Positive-sequence voltage magnitude at PCC, (b) output power at the inverter terminal, (c) three-phase currents at the inverter terminal.

TABLE 1
IMPEDANCE ANGLES UNDER DIFFERENT FAULT LOCATIONS AND TYPES

Relay	Fault points	Fault types	$\angle Z_1$	$\angle Z_2$
R_{12}	F1	BG	79.19	79.20
		AB	79.27	79.27
		BCG	79.21	79.46
		ABCG	79.28	/
R_{12}	F2	BG	-90.69	-88.87
		AB	-90.65	-89.49
		BCG	-90.77	-88.90
		ABCG	-90.66	/
R_{12}	F3	BG	-90.79	-88.61
		AB	-90.66	-89.50
		BCG	-90.78	-88.75
		ABCG	-90.92	/
R_{12}	F4	BG	-90.98	-89.88
		AB	-90.68	-90.08
		BCG	-91.06	-89.33
		ABCG	-90.92	/
R_{21}	F5	BG	88.55	89.74
		AB	88.92	89.13
		BCG	88.88	89.97
		ABCG	88.72	/

0 Ω, and the simulation results are illustrated in Table 1. All the values in the table are taken from 100 ms after the fault inception. The letters A, B and C represent faulty phases, and G means phase to ground.

It can be seen from Table 1 that both positive- and negative-sequence directional elements at R_{12} can detect an impedance angle close to -90° for forward faults, so their sensitivity is improved regardless of fault points and fault types. This proves that this new control method has an excellent regulation effect on the sequence impedance angles of CIRESs. For reverse faults at F1, the impedance angle calculated at R_{12} reflects the impedance feature of the transmission line and the equivalent grid, so a reverse fault can always be identified. During bolted three-phase faults, the proposed method fixes the output frequency of the phase-locked loop (PLL) at the fundamental frequency, so the output fault current from CIRESs is still power frequency such that the proposed control method is still effective. However, considering that the power transfer will stop for this type of fault, some grid-following inverters may not output the stable fundamental-frequency fault current. In this case, the proposed control method will not work properly. In addition, For the grid-side relay R_{21}, the impedance angles seen by positive- and negative-sequence directional elements are close to 90° for reverse faults at F5, so the direction can be also detected correctly.

C. Case study with different fault resistances

In this section, the proposed control scheme is simulated under various fault resistances. For the 220 kV transmission line, a 100 Ω coverage is usually enough for most cases [19, 33], so the fault resistance is set to 0 Ω, 50 Ω, and 100 Ω, respectively. The impedance angles detected by positive- and negative-sequence directional elements at R_{12} are
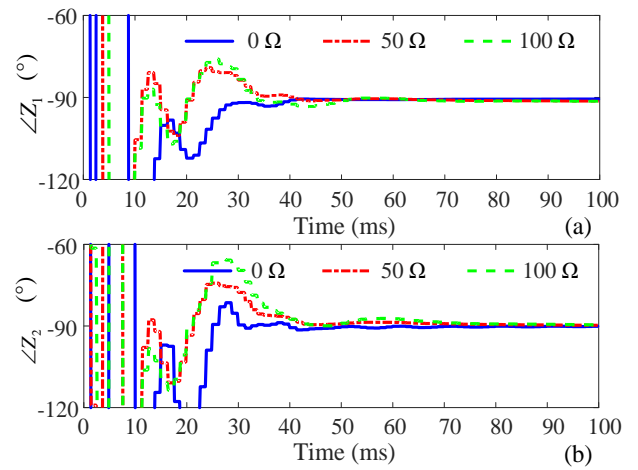

Fig. 9. The performance of directional elements under different fault resistances for AG faults at F3. (a) $\angle Z_1$, (b) $\angle Z_2$.

displayed in Fig. 9 when an AG fault arises at F3.

As seen in Fig. 9 (a), the impedance angle measured by positive-sequence directional elements is -91.33° for 50 Ω and -91.38° for 100 Ω, and the deviation from -90° is so small that the directional element has high sensitivity. In addition, the impedance angles measured by negative-sequence directional elements in Fig. 9 (b) are basically equal in three cases, thus the performance of negative-sequence directional elements is not adversely affected by the fault resistance.

D. Case study with weak grid operation

This section evaluates the proposed control scheme under an operation in a weak grid. The grid is weakened by increasing the grid impedance to 1.0+j34.85 Ω and 13.32+j131.88 Ω so that the CIRES capacity is respectively one-tenth and one-third of the grid short-circuit capacity measured at R_{12}. When a metallic AB fault occurs at F3 at 0 s, the impedance angles detected by directional elements at R_{12} are depicted in Fig. 10.

It can be seen from Fig. 10 that the impedance angles measured by directional elements at R_{12} are very similar when the CIRES capacity is respectively equal to one-thirtieth and one-tenth of the short-circuit capacity of the grid. However, the apparent impedance will have some differences from the above two situations when this ratio is increased to one-third, but this does not affect the accuracy of direction detection, which illustrates the effectiveness of the proposed method.
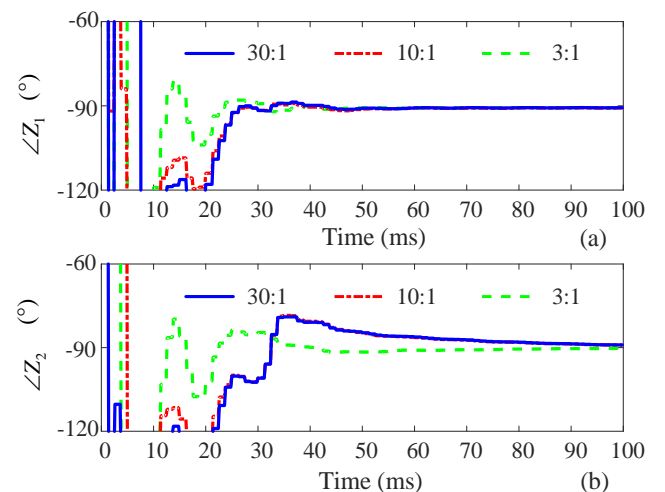

Fig. 10. The performance of elements in weak grids. (a) $\angle Z_1$, (b) $\angle Z_2$.
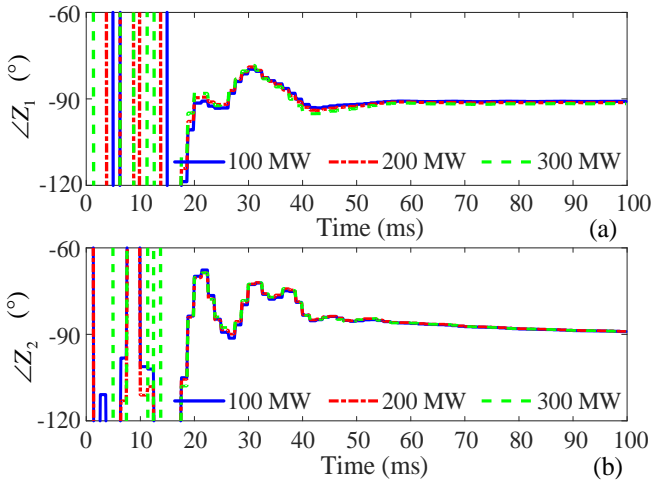
Fig. 11. The performance of directional elements under different power rates. (a) $\angle Z_1$, (b) $\angle Z_2$.

E. Case study with different power ratings

The CIRES capacity is increased to 200 MW and 300 MW, respectively. In this case, the impedance angles detected by two directional elements at R_{12} are displayed in Fig. 11 for a bolted BC fault at F4.

All the impedance angles measured by positive-sequence directional elements in Fig. 11 (a) are close to -90°, so the proposed control scheme is also not affected by power ratings. The reason is that the proposed method can adjust the output fault current angle according to the actual measurements. In addition, a similar phenomenon can be observed in Fig. 11 (b) for negative-sequence directional elements.

F. Comparison case with other control-based methods

The positive-sequence fault circuit of CIRESs can be controlled to a constant voltage source with a constant impedance by the method in [22]. However, the impedance angle seen by positive-sequence directional elements cannot be adjusted by this method because it is related to the electric components before the fault. In order to compare these two methods, the power factors before the fault are respectively set to 0.9, 0.95 and 1. At this time, the impedance angle detected by positive-sequence directional elements at R_{12} is shown in Fig. 12 when BC faults with 20 Ω of fault resistance appear at F3.

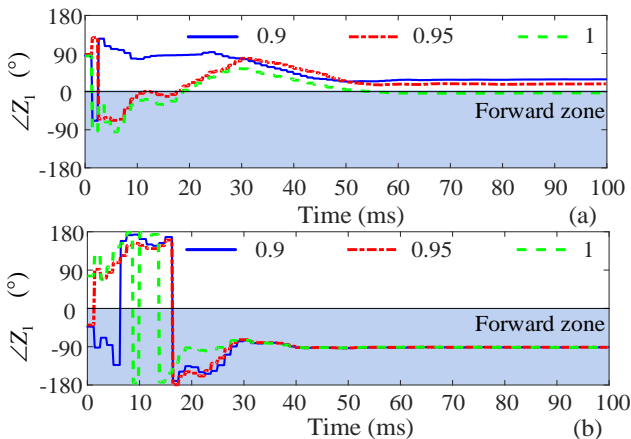As seen in Fig. 12 (a), the impedance angle detected by

Fig. 12. The performance of positive-sequence elements under two control methods. (a) The method in [22], (b) the proposed method.
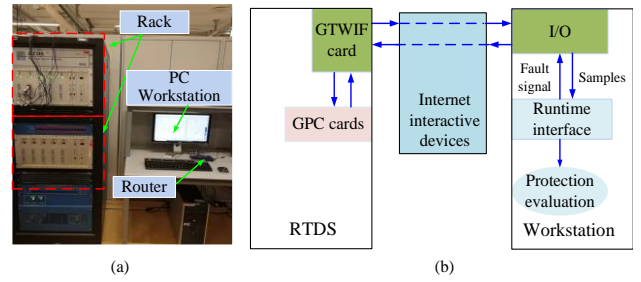

(a) (b)

Fig. 13. The experiment platform based on RTDS. (a) Hardware devices, (b) hardware topology.

positive-sequence directional elements is affected by the power factor before the fault when the method in [22] is performed. Especially when the power factor is 0.9 and 0.95, the elements even misjudge the fault direction. However, the proposed method can make the apparent impedance angle close to -90° under different power factors before the fault, as shown in Fig. 12 (b).

V. RTDS VALIDATION

The proposed method is also validated by real-time simulations performed in RTDS as depicted in Fig. 13. The RTDS platform includes two Racks, an internet router, and a PC workstation. The Rack is the basic unit of the RTDS, which is composed of different RTDS cards and an internet switch. Among them, GPC cards have a high running speed, and they are used to perform the established model (the same as that in PSCAD) in RSCAD which is a special environment for RTDS devices. Furthermore, the generated data in GPC cards will be returned to the PC workstation by a GTWIF card in a local area network that includes an internet switch and a router. Finally, the protection performance is verified by MATLAB programming.

When an AG fault with 100 Ω of fault resistance and a BC fault with 20 Ω of fault resistance occur at F4, three-phase fault currents from CIRESs for this AG fault and impedance angles detected by directional elements at R_{12} for two faults can be observed in Fig. 14.

As depicted in Fig. 14 (a), three-phase fault currents are always lower than the current limiting value. At this time, the impedance angle measured by positive-sequence
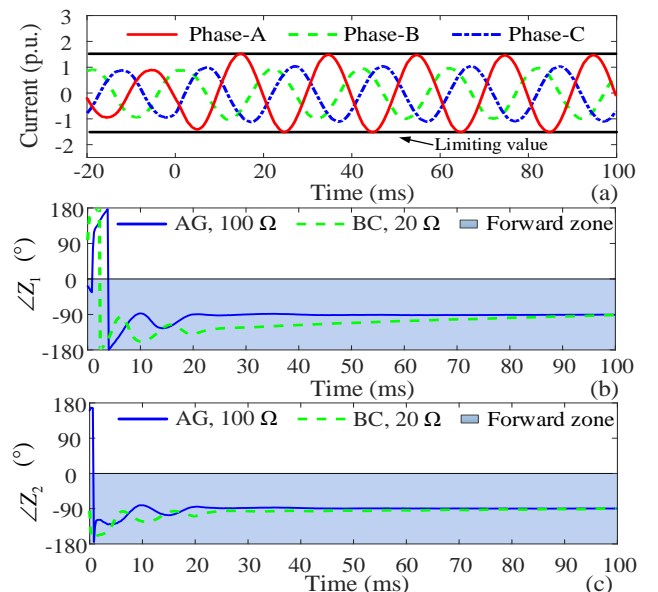

Fig. 14. Three-phase fault currents from CIRESs and the performance of directional elements. (a) Three-fault currents, (b) $\angle Z_1$, (c) $\angle Z_2$.

directional elements in Fig. 14 (b) is equal to -90.65° for an AG fault with 100 Ω of fault resistance and -91.36° for a BC fault with 20 Ω of fault resistance, so positive-sequence directional element can work properly. In addition, the impedance angles detected by negative-sequence directional elements also approach -90° for these two cases in Fig. 14 (c). These results show this new control method is effective to improve the performance of directional elements as well.

VI. DOWNSCALE HARDWARE EXPERIMENT

Finally, a downscale hardware experiment is performed based on an actual inverter in Fig. 15 (a). The inverter is connected to DY_n11 transformer with a transfer ratio of 1:1 by an L power filter, as observed in Fig. 15 (b). Since the DC voltage participates in the generation of the modulation wave, the transient process of the DC voltage will not affect the fault characteristics of the AC side. Therefore, a constant DC voltage source can be used to substitute the DC capacitor in the experiment [34]. Although traditional directional elements should collect the voltage and current data from the high-voltage side of the transformer, the main function of the proposed control method is to adjust the source impedance angle, so it is acceptable to test the performance of the proposed method by collecting the current and voltage signals on both sides of the filter. Since the transformer has different connection wirings on the low-voltage and high-voltage sides, sequence voltages and currents on the high-voltage side will have an angle difference from their corresponding components on the low-voltage side. However, all positive-sequence voltages and currents on the high-voltage side will be rotated in the same direction, so the apparent impedance angle detected by positive-sequence directional elements on the high-voltage side will be basically equal to that on the low-voltage side. The apparent impedance angle of negative-sequence directional elements is the same case. In addition, a real grid fault is not possible to create in a laboratory environment, so it is substituted by a voltage sag produced by a three-phase power source *California Instruments MX-35* [35]. In addition, the
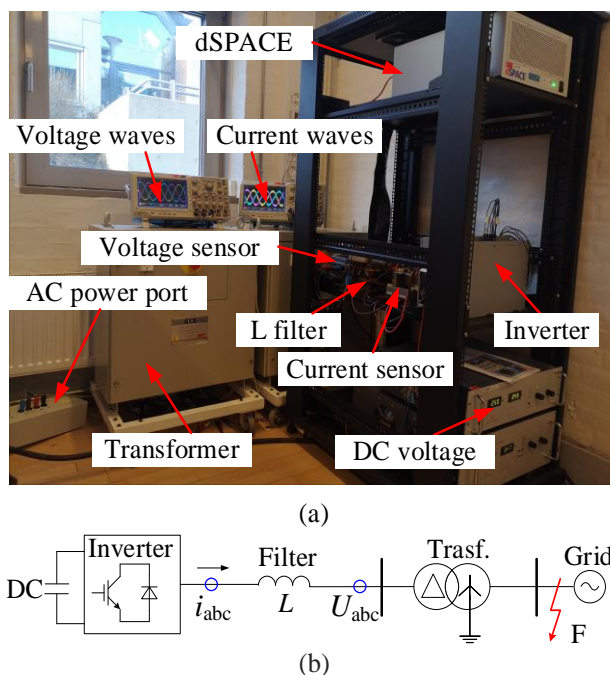

(a)

(b)

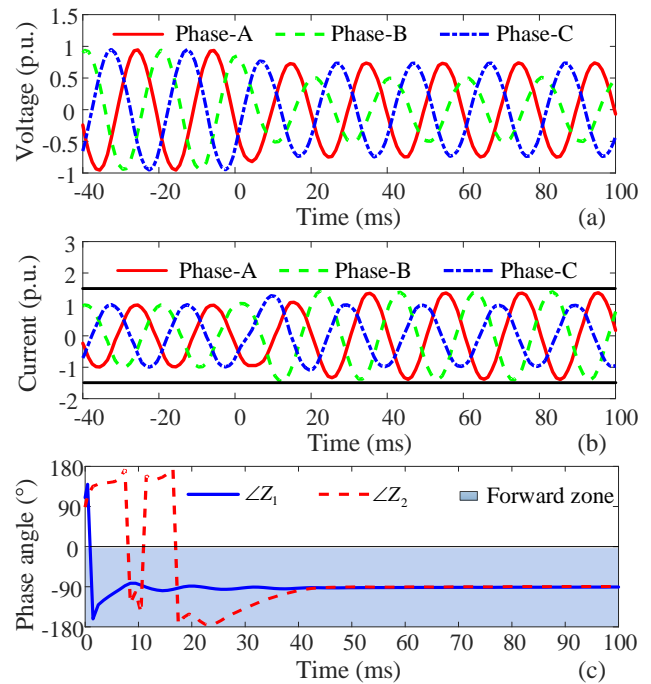Fig. 15. Physical experiment platform. (a) Hardware devices, (b) hardware topology.

Fig. 16. The output fault current from the inverter for a given voltage drop. (a) The measured voltage, (b) the fault current, (c) impedance angle.

controller of the inverter is constructed in the dSPACE, and the specific hardware parameters are shown in Table A.II.

When a voltage drop of 0.5 p.u. for phase-A and phase-B is generated by *MX-35*, the measured voltage, the measured current, and the apparent impedance angle are given in Fig. 16 after the proposed control method is performed.

As shown in Fig. 16 (a), the measured voltage presents a different magnitude feature from the applied voltage by MX-35 at F due to the wiring mode of the transformer, and the voltage sag appears at 0 s. At this time, the fault current of phase-B from the inverter in Fig. 16 (b) can reach the maximum current limiting value and reach the steady state within 40 ms. Under this circumstance, the impedance angles in Fig. 16 (c) measured by positive- and negative-sequence directional elements are close to -90°, so they can detect a forward fault with high sensitivity, which strongly supports the proposed control method once again.

VII. DISCUSSION

The proposed control method is aimed to enhance the performance of directional elements, but still has some shortcomings that need to be solved in the future:

1) The stability of a system with multiple controllers of various kinds is outside of the scope of this paper, and this document does not provide the proof of stability.

2) The proposed method is applied for fault scenarios where positive- and negative-sequence components are decoupled. Therefore, its performance needs to be further studied especially in cases where the sequence components are not decoupled.

3) The method is only applicable to sources that are not installed near large clusters of Type III wind generators.

4) i_{1qref} is no longer set according to voltage sags, so the effect of the proposed method on voltage transients needs to be further investigated.

Although the proposed control scheme still has some open issues, it is a promising method to make CIRESs compatible with directional elements of line protection.

VIII. Conclusions

The traditional fault control strategy of CIRESs will lead to a variable sequence impedance angle for CIRESs, so directional elements of line protection may fail to operate.

In order to solve this issue, the impedance angles detected by the directional elements are restored to -90° by designing the suitable fault current angle output from CIRESs. Meanwhile, the maximum allowable fault current is reached by an iterative algorithm to make full use of the CIRES short-circuit capacity. When the proposed control scheme is performed, CIRESs can be compatible with traditional directional elements, so these directional elements can operate correctly. In addition, all the parameters of the controller are not necessary to be revised according to different fault types, and only the local data are used. Simulation results in PSCAD, RTDS experiment, and downscale hardware experiment have demonstrated that the proposed method can perform well for different fault types and other various fault scenarios while the important FRT requirements can still be satisfied.

In the future, hardware-in-the-loop (HIL) testing will be performed to verify the proposed method further.

Appendix

Table A.I
Simulation Parameters

Element	Parameter	Value
Transmission line	Positive-sequence impedance	$0.076+j0.338\ \Omega/km$
	Zero-sequence impedance	$0.284+j0.824\ \Omega/km$
	Positive-sequence capacitance	$0.0086\ \mu F/km$
	Zero-sequence capacitance	$0.0061\ \mu F/km$
LCL filter	Capacitor (C)	$220\ \mu F$
	Inductance (L_1 and L_2)	$1250/1250\ \mu H$
	Resistance (R)	$0.01\ \Omega$
Main transf.	Rated capacity	100 MVA
	Rated transformation ratio	220/35 kV
	Wire connection	YNd
	Short circuit impedance	10%
Step-up transf.	Rated capacity	1.6 MW
	Rated transformation ratio	0.38/35 kV
	Wire connection	Dyn
	Short circuit impedance	6%
Collection line	Equivalent impedance	$0.11+j0.157\ \Omega$
DC bus	Rated voltage	2 kV
	DC capacitance (C_d)	$7800\ \mu F$
	Chopper resistance (R_d)	$0.5\ \Omega$

Table A.II
Hardware Parameters

Parameters	Values
Rated grid voltage	190 V
Rated capacity	2.5 kVA
DC voltage	500 V
System frequency	50 Hz
The power filter resistance	$62\ m\Omega$
The power filter inductance	4.2 mH
Switching frequency	10 kHz
Sampling frequency	1 kHz
dSPACE processor board	DS1006
dSPACE digital IO board	DS5101

References

[1] D. V. Bozalakov, T. L. Vandoorn, B. Meersman, G. K. Papagiannis, A. I. Chrysochos and L. Vandevelde, "Damping-Based Droop Control Strategy Allowing an Increased Penetration of Renewable Energy Resources in Low-Voltage Grids," in *IEEE Trans. Power Del.*, vol. 31, no. 4, pp. 1447-1455, Aug. 2016.

[2] W. Cui, Y. Jiang and B. Zhang, "Reinforcement Learning for Optimal Primary Frequency Control: A Lyapunov Approach," in *IEEE Trans. Power Systems*.

[3] K. Jia, Q. Liu, B. Yang, L. Zheng, Y. Fang and T. Bi, "Transient Fault Current Analysis of IIRESs Considering Controller Saturation," in *IEEE Trans. Smart Grid*, vol. 13, no. 1, pp. 496-504, Jan. 2022.

[4] A. K. Pradhan and P. Jena, "Solution to Close-in Fault Problem in Directional Relaying," in *IEEE Trans. Power Del.*, vol. 23, no. 3, pp. 1690-1692, July 2008.

[5] V. Telukunta, J. Pradhan, A. Agrawal, M. Singh and S. G. Srivani, "Protection challenges under bulk penetration of renewable energy resources in power systems: A review," in *CSEE J. Power Energy Syst.*, vol. 3, no. 4, pp. 365-379, Dec. 2017.

[6] Jisi Tang, Guobing Song, Xiaobo Wang and Chenqing Wang, "A novel directional relay applicable to power system with wind farms," *2016 IEEE PES Asia-Pacific Power and Energy Engineering Conference (APPEEC)*, 2016, pp. 2117-2121.

[7] Y. Chen, M. Wen, L. Hu, X. Qi, J. Zheng and Z. Wang, "Fault direction identification for wind power integration system," in *The Journal of Engineering*, vol. 2019, no. 16, pp. 2520-2524, 3 2019.

[8] J. Tang, G. Song and C. Wang, "Adaptability analysis of directional relays in power systems with wind farms," *13th International Conference on Development in Power System Protection 2016 (DPSP)*, Edinburgh, 2016, pp. 1-6.

[9] K. Jia, Z. Yang, Y. Fang, T. Bi and M. Sumner, "Influence of Inverter-Interfaced Renewable Energy Generators on Directional Relay and an Improved Scheme," in *IEEE Trans. Power Electron.*, vol. 34, no. 12, pp. 11843-11855, Dec. 2019.

[10] A. Hooshyar and R. Iravani, "A New Directional Element for Microgrid Protection," in *IEEE Trans. Smart Grid*, vol. 9, no. 6, pp. 6862-6876, Nov. 2018.

[11] A. Haddadi, M. Zhao, I. Kocar, U. Karaagac, K. W. Chan and E. Farantatos, "Impact of Inverter-Based Resources on Negative Sequence Quantities-Based Protection Elements," in *IEEE Trans. Power Del.*, vol. 36, no. 1, pp. 289-298, Feb. 2021.

[12] R. Chowdhury and N. Fischer, "Transmission Line Protection for Systems with Inverter-Based Resources – Part I: Problems," in *IEEE Trans. Power Del.*, vol. 36, no. 4, pp. 2416-2425, Aug. 2021.

[13] C. Wang, G. Song, et al, "A novel principle of directional relay for wind power integration based on model recognition in time-domain," *2016 IEEE PES Asia-Pacific Power and Energy Engineering Conference (APPEEC)*, Xi'an, 2016, pp. 1851-1855.

[14] G. Suryanarayana, G. Kesava Rao, et al, "Directional relaying using parameter estimation approach," in *Int. J. of Electr. Power Energy Syst*, vol. 107, pp. 597-604, 2019.

[15] X. Wang, M. Wen, et al, A novel directional relay for AC lines close to the HVDC installation, in *Int. J. of Electr. Power Energy Syst*, vol. 118: pp. 105726, 2020.

[16] H. Jafarabadi Ashtiani, H. Samet and T. Ghanbari, "Evaluation of directional relay algorithms in the presence of FCL," in *IET Science, Measurement & Technology*, vol. 11, no. 6, pp. 713-722, Sep. 2017.

[17] H. Li, J. Duan, Y. Lei and L. Tuo, "Ultra-high-speed transient-based directional relay for AC transmission lines connected to LCC-HVDC inverter station," in *Int. J. of Electr. Power Energy Syst*, vol. 123: pp. 106235, 2020.

[18] Ma, K., et al., "Protection collaborative fault control for power electronic-based power plants during unbalanced grid faults," in *Int. J. of Electr. Power Energy Syst.,* vol.130, pp. 107009, 2021.

[19] R. Chowdhury and N. Fischer, "Transmission Line Protection for Systems With Inverter-Based Resources – Part II: Solutions," in *IEEE Trans. Power Del.*, vol. 36, no. 4, pp. 2426-2433, Aug. 2021.

[20] M. A. Azzouz, A. Hooshyar and E. F. El-Saadany, "Resilience Enhancement of Microgrids With Inverter-Interfaced DGs by Enabling Faulty Phase Selection," in *IEEE Trans. Smart Grid*, vol. 9, no. 6, pp. 6578-6589, Nov. 2018.

[21] A. Haddadi, I. Kocar, J. Mahseredjian, U. Karaagac and E. Farantatos, "Negative sequence quantities-based protection under inverter-based resources Challenges and impact of the German grid code," *in Electr. Power Syst. Res.*, vol. 188, no. 6, pp. 106573, July 2020.

[22] A. Banaiemoqadam, A. Hooshyar and M. A. Azzouz, "A Comprehensive Dual Current Control Scheme for Inverter-Based Resources to Enable Correct Operation of Protective Elements," in *IEEE Trans. Power Del.*, vol. 36, no. 5, pp. 2715-2729, Oct. 2021.

[23] A. Hooshyar, E. F. El-Saadany and M. Sanaye-Pasand, "Fault Type Classification in Microgrids Including Photovoltaic DGs," in *IEEE Trans. Smart Grid*, vol. 7, no. 5, pp. 2218-2229, Sept. 2016.

[24] Hong-Seok Song and Kwanghee Nam, "Dual current control scheme for PWM converter under unbalanced input voltage conditions," in *IEEE Trans. Ind. Electron.*, vol. 46, no. 5, pp. 953-959, Oct 1999.

[25] J. Svensson, M. Bongiorno and A. Sannino, "Practical Implementation of Delayed Signal Cancellation Method for Phase-

Sequence Separation," in *IEEE Trans. Power Del.*, vol. 22, no. 1, pp. 18-26, Jan. 2007.

[26] A. Banaiemoqadam, A. Hooshyar and M. A. Azzouz, "A Control-Based Solution for Distance Protection of Lines Connected to Converter-Interfaced Sources During Asymmetrical Faults," in *IEEE Trans. Power Del.*, vol. 35, no. 3, pp. 1455-1466, June 2020.

[27] Wang, P., Song, J., Liang, F. *et al,* " Equivalent model of multi-type distributed generators under faults with fast-iterative calculation method based on improved PSO algorithm, "*Prot. Control Mod. Power Syst.*, 2021.

[28] K. Jia, Y. Li, et al., "Transient Current Similarity Based Protection for Wind Farm Transmission Lines, " in *Applied Energy*, vol. 225, pp. 42-51, Sep. 2018.

[29] P. Piya, M. Ebrahimi, M. Karimi-Ghartemani and S. A. Khajehoddin, "Fault Ride-Through Capability of Voltage-Controlled Inverters," in *IEEE Trans. Ind. Electron.*, vol. 65, no. 10, pp. 7933-7943, Oct. 2018.

[30] H. Guo, "Sequence-Impedance Modeling of Voltage Source Converter Interconnection Under Asymmetrical Grid Fault Conditions," in *IEEE Trans. Ind. Electron.*, vol. 68, no. 2, pp. 1332-1341, Feb. 2021.

[31] L. Harnefors, M. Bongiorno and S. Lundberg, "Input-Admittance Calculation and Shaping for Controlled Voltage-Source Converters," in *IEEE Trans. Ind. Electron.*, vol. 54, no. 6, pp. 3323-3334, Dec. 2007.

[32] J.J. Chavez, M. Popov, D. López, S. Azizi and V. Terzija, "S-Transform based fault detection algorithm for enhancing distance protection performance," in *Int. J. of Electr. Power Energy Syst.*, vol. 130, pp. 106966, 2021.

[33] L. Zheng, K. Jia, T. Bi, and et al, "A Novel Structural Similarity Based Pilot Protection for Renewable Power Transmission Line," in *IEEE Trans. Power Del.*, vol. 35, no. 6, pp. 2672-2681, Dec. 2020.

[34] Q. Zhang, D. Liu, Z. Liu and Z. Chen, "Fault Modeling and Analysis of Grid-connected Inverters with Decoupled Sequence Control," in *IEEE Trans Ind. Electron*, vol. 69, no. 6, pp. 5782-5792, June 2022.

[35] MX Series AC and DC Power Source, Installation Manual Rev: D [online]. Available: https://www.programmablepower.com/products/ac-power-sources/mx-series.

Zhe Yang (Student Member, IEEE) was born in China in 1994. He received the bachelor's degree in electrical engineering from the Northeast Electric Power University in 2017, and the master's degree in electrical engineering with North China Electric Power University in 2020.

He is currently pursuing Ph.D. degree in AAU Energy with Aalborg University. His research interest is power system protection and control.

Zhou Liu (Senior Member, IEEE) received the Ph.D. degree from Department of Energy Technology, Aalborg University, Denmark, in 2013. He worked as an Assistant Professor at the Department of Energy Technology, Aalborg University, Denmark (2018-2021). He is currently a Research Professional in Siemens Gamesa. His research interests include Wind Power integration, Power system modelling and simulation, Power system stability, protection and control, smart grid and AI technology.

Qi Zhang (Student Member, IEEE) received the B.Eng and M.Sc in electrical engineering from China University of Mining and Technology (Beijing), Beijing, China, in 2015 and 2018, respectively. Currently, he is working towards Ph.D. in AAU Energy with Aalborg University.

His main research interests include fault analysis of the power electronic dominated power system, modeling and control of the power system.

Zhe Chen (Fellow, IEEE) received the B.Eng. and M.Sc. degrees from the Northeast China Institute of Electric Power Engineering, Jilin City, China, in 1982 and 1986, and the Ph.D. degree from the University of Durham, U.K., in 1997. Dr. Chen is a Full Professor with the Department of Energy Technology, Aalborg University, Denmark. He is the Leader of Wind Power System Research program at the Department of Energy Technology, Aalborg University and the Danish Principle Investigator for Wind Energy of Sino-Danish Centre for Education and Research. His research areas are power systems, power electronics and electric machines, and his main current research interests are wind energy and modern power systems. He has led many research projects and has more than 500 publications in his technical fields.

Jose de Jesus Chavez (Member, IEEE) received the M.Sc. and Ph.D. degrees from the Center for Research and Advanced Studies, National Polytechnic Institute, Mexico City, in 2006 and 2009, respectively. In 2009, he joined the RTX-LAB, University of Alberta, as a Visiting Ph.D. Student. He joined the Technological Institute of Morelia, Mexico, as an Assistant Professor in 2010, where he was a Full Professor in 2012 and the Chair of the Graduate and Research Program in electrical engineering from 2014 to 2016. He was a Post-Doctoral Member with TU Delft, The Netherlands 2016-2020 and guest researcher since 2021. Currently, he is a Professor at The National Technological Institute of Mexico (TecNM). His research interests include primary protection, wide area protection, digital protective relays, and real-time simulation.

Marjan Popov (M'95, SM'03, F'22) obtained his Ph.D. degree in electrical power engineering from Delft University of Technology, Delft in 2002. He is also a Chevening Alumnus and, in 1997, he was an Academic Visitor with the University of Liverpool, Liverpool, U.K., working in the Arc Research Group on modeling SF6 circuit breakers. His major fields of interest are in future power systems, large-scale power system transients, intelligent protection for future power systems, and wide-area monitoring and protection. He is a member of Cigre and actively participated in WG C4.502 and WG A2/C4.39. In 2010, he received the prestigious Dutch Hidde Nijland Prize for extraordinary research achievements. He was the recipient of the IEEE PES Prize Paper Award and IEEE Switchgear Committee Award in 2011 and an Associate Editor for Elsevier's International Journal of Electrical Power and Energy Systems. In 2017, together with the Dutch utilities TenneT, Alliander and Stedin he founded the Dutch Power System Protection Centre to promote the research and education in power system protection.